

# Creep motion of elastic interfaces driven in a disordered landscape

E. E. Ferrero,<sup>1</sup> L. Foini,<sup>2</sup> T. Giamarchi,<sup>3</sup> A. B. Kolton,<sup>4</sup> and A. Rosso<sup>5</sup>

<sup>1</sup>Instituto de Nanociencia y Nanotecnología, Centro Atómico Bariloche, CNEA-CONICET, R8402AGP San Carlos de Bariloche, Río Negro, Argentina

<sup>2</sup>IPhT, CNRS, CEA, Université Paris-Saclay, 91191 Gif-sur-Yvette, France

<sup>3</sup>Department of Quantum Matter Physics, University of Geneva, 24 Quai Ernest-Ansermet, CH-1211 Geneva, Switzerland

<sup>4</sup> Instituto Balseiro, Centro Atómico Bariloche, CNEA-CONICET-UNCUYO, R8402AGP San Carlos de Bariloche, Río Negro, Argentina

<sup>5</sup>LPTMS, CNRS, Univ. Paris-Sud, Université Paris-Saclay, 91405 Orsay, France

Xxxx. Xxx. Xxx. Xxx. YYYY. AA:1–25

[https://doi.org/10.1146/\(\(please add article doi\)\)](https://doi.org/10.1146/((please add article doi)))

Copyright © YYYY by Annual Reviews.  
All rights reserved

## Keywords

creep, domain walls, depinning, disordered elastic systems, avalanches, activated motion

## Abstract

The thermally activated creep motion of an elastic interface weakly driven on a disordered landscape is one of the best examples of glassy universal dynamics. Its understanding has evolved over the last 30 years thanks to a fruitful interplay between elegant scaling arguments, sophisticated analytical calculations, efficient optimization algorithms and creative experiments. In this article, starting from the pioneer arguments, we review the main theoretical and experimental results that lead to the current physical picture of the creep regime. In particular, we discuss recent works unveiling the collective nature of such ultra-slow motion in terms of elementary activated events. We show that these events control the mean velocity of the interface and cluster into “creep avalanches” statistically similar to the deterministic avalanches observed at the depinning critical threshold. The associated spatio-temporal patterns of activated events have been recently observed in experiments with magnetic domain walls. The emergent physical picture is expected to be relevant for a large family of disordered systems presenting thermally activated dynamics.

## Contents

|   |    |
|---|----|
| 1. Introduction .....   | 2  |
| 2. Dynamical phase diagram at zero temperature.....                     | 3  |
| 2.1. The case of the quenched Kardar-Parisi-Zhang (KPZ) depinning ..... | 7  |
| 3. Velocity at finite temperature.....                                  | 8  |
| 4. Numerical methods.....   | 11 |
| 5. Creep dynamics in the limit of vanishing temperature .....           | 12 |
| 5.1. Statistics of the events and clusters .....                        | 13 |
| 5.2. Geometry of the interface.....                                     | 14 |
| 5.3. Optimal Paths and Barriers.....                                    | 16 |
| 6. Comparison with Experiments .....                                    | 18 |
| 6.1. Creep Velocity.....  | 18 |
| 6.2. The Roughness puzzle .....   | 19 |
| 6.3. Creep avalanches .....   | 21 |
| 7. Conclusions and Perspectives .....                                   | 22 |

### 1. Introduction

Our understanding of physics is largely based on idealized problems, the famous ‘spherical cows’. Yet, the beauty of nature makes use of a much vast complexity. It is well known nowadays that the presence of impurities and defects messing up with those rounded mammals leads to new emerging physical behavior, not observed in the idealized disorder-free problems. For example, the equilibration time of glasses becomes so large that it results to be experimentally inaccessible. Such systems avoid crystallization and basically live forever out-of-equilibrium (1, 2). Dirty metals display localization and metal insulator transitions, unseen in perfect crystals (3, 4). Systems of a broadly diverse nature show intermittent dynamics induced by the presence of disorder (5). Strained amorphous materials (6, 7, 8), fracture fronts (9, 10, 11), magnetic (12, 13) and ferroelectric domain walls (14, 15), liquid contacts lines (16, 17), they all share a common phenomenology: when the applied drive is just enough to induce motion, most of the system remains pinned but large regions move collectively at high velocity. These reorganizations are called avalanches. Their location is typically unpredictable and their size distribution display a scale free statistics. Given the ubiquity of this stick-slip behavior, the study avalanches has occupied a central scene in non-equilibrium statistical physics, as can be seen in the large literature of sandpile models (18), directed percolation and cellular automata (19).

The depinning of an elastic interface moving in a disordered medium (20, 21, 22, 23, 24, 25) is one of the paradigmatic examples where avalanches are well understood, thanks to the analogy with standard equilibrium critical phenomena (22, 26). When the interface is driven at the force  $f$  two phases are generically observed: for  $f < f_c$  the interface is pinned at zero temperature and motion is observed only during a transient time, for  $f > f_c$  the line moves with a finite steady velocity. At  $f_c$  the system displays a dynamical phase transition and the diverging size of avalanches is the outcome of the presence of critical correlations. Below and above  $f_c$  the avalanches display a finite cut-off, that diverges approaching  $f_c$ . We presently know the statistics of avalanches sizes (27) and durations (28) and their characteristic shape (29, 30). An important observation is that subsequent depinning avalanches are uncorrelated in space and time at variance with the avalanche behavior observed in many

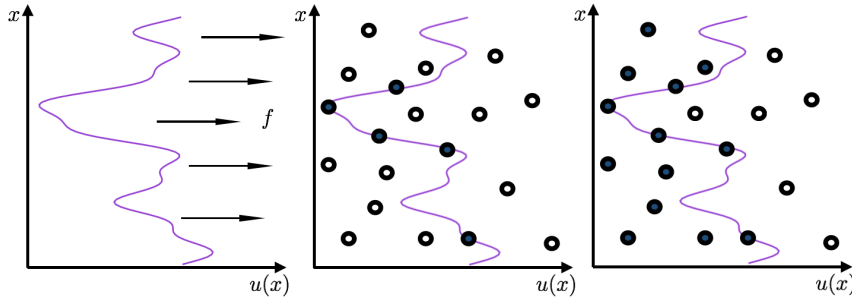


Figure 1: *Left*: Sketch of the interface pulled by an external force  $f$ . The dark circles are the impurities that contribute to the pinning energy of the interface. In the random bond case (*center*) only neighboring impurities contribute while in the random field case (*right*) all the impurities on the left side of the interface contribute.

systems where a ‘main-shock’ is at the origin of a cascade of ‘after-shocks’. The so-called Omori law and productivity law, central in the geophysics of earthquakes (31), are not present at the depinning transition<sup>1</sup>. Namely all the experimental observations of depinning avalanches temporally correlated were shown to be related to a finite detection threshold, created by the limited sensitivity of the measurement apparatus (34).

Nonetheless, genuine aftershocks could be experimentally observed far from the depinning transition, in the so-called *creep* regime. This regime, which describes the motion of magnetic domain walls at finite (e.g. room) temperature and low applied fields, corresponds to an interface pulled by a small force ( $f \ll f_c$ ) at finite temperature (35, 24, 25). The collective dynamics observed in this case is qualitatively different from the one at the critical threshold. In both regimes the dynamics is collective and involves large scale reorganizations. But from the more recent results creep ‘‘avalanches’’ display complex spatio-temporal patterns similar to the ones of observed in earthquakes.

In this paper we review the main arguments and results of the last thirty years about creep with particular attention to the recent progress. The paper is organized as follows. In Sect. 2 we introduce the model, present the dynamical regimes at zero temperature and discuss the different universality classes. In Sect. 3 we provide the scaling arguments leading to the creep law, namely the behavior of the steady velocity as a function of the applied force at finite temperature. The numerical methods are discussed in Sect. 4. The more recent results valid in the limit of vanishing temperature are presented in Sect. 5. In Sect. 6 we review the creep experiments on domain wall dynamics. Conclusions and perspectives are given in Sect. 7.

## 2. Dynamical phase diagram at zero temperature

We consider a  $d$ -dimensional interface in a  $d + 1$  disordered medium. For simplicity we assume that the local displacement at any time  $t$  is described by a single valued function  $u(x, t)$  (see **Figure 1 left**) and that the dynamics is overdamped. At zero temperature the

<sup>1</sup>Although depinning-inspired models have been adapted to produce aftershocks by adding terms of slow relaxation or memory (32, 33)

equation of motion of the elastic manifold writes:

$$\gamma \partial_t u(x, t) = c \nabla^2 u(x, t) + f + F_p(x, u) \quad 1.$$

where  $c \nabla^2 u(x, t)$  describes the elastic force due to the surface tension,  $f$  is the external pulling force and  $\gamma$  the microscopic friction. The fluctuations induced by impurities are encoded in the quenched stochastic term  $F_p = -\partial_u V_p(x, u)$ , where the energy potential  $V_p(x, u)$  describes the coupling between the manifold and the impurities.

For simplicity we assume the absence of correlations along the  $x$  direction <sup>2</sup>, while the correlations of  $V_p(x, u)$  along the  $u$  direction usually belong to one of two universality classes: (i) In the Random Bond class (RB) the impurities affect in a symmetric way the phases on each side of the interface. They thus simply locally attract or repel the interface (see **Figure 1 center**). In this case the pinning potential and the pinning force are both short-ranged correlated. (ii) The Random Field class (RF) describes a disorder coupling in a different way in the two phases around the interface. Thus the pinning energies are affected by the impurities inside the entire region delimited by the interface (see **Figure 1 right**). Then  $F_p$  displays short range correlations while the pinning potential  $V_p(x, u)$  displays long-range correlations  $[\overline{V_p(x, u) - V_p(x', u')}]^2 \propto \delta(x - x') |u - u'|$ . Here, the overline denotes average over disorder realizations.

Equation Eq.1, so called quenched Edwards-Wilkinson equation, is a coarse-grained minimal model governing the dynamics of the interface, at zero temperature for the moment, at large scales (22, 26, 25). It is a non-linear equation in  $u$  that has been extensively studied by numerical simulation (37), functional renormalization group techniques (FRG) (38, 21, 39) and exact mean-field solutions (40, 41, 42). For the case of a contact line of a liquid meniscus (43) as well as the crack front of a brittle material (44) the local elastic force is replaced by a long range one:

$$c \nabla^2 u \rightarrow c \int \frac{(u(x', t) - u(x, t))}{|x' - x|^{\alpha+d}} d^d x' \quad 2.$$

with  $\alpha = 1$  and  $d = 1$ . The qualitative phenomenology of this generalized long range model is similar to the quenched Edwards-Wilkinson, but the universal properties (as critical exponents and scaling functions) are different. However, for  $\alpha \geq 2$  one recovers the short-range universality class (45).

The solution of this class of equations shows a behavior reminiscent of second order phase transitions with the velocity playing the role of the order parameter and the force acting as the control parameter. In particular, below a critical *depinning* threshold  $f_c$  the steady velocity is zero, and it acquires a finite value above only above that threshold. The velocity vanishes continuously at the critical force as  $v \simeq (f - f_c)^\beta$ . At the depinning the interface appears rough with a width

$$w^2(L) = \frac{1}{L} \int_0^L u^2(x) dx - \left( \frac{1}{L} \int_0^L u(x) dx \right)^2 \quad 3.$$

that grows as  $L^{2\zeta_{\text{dep}}}$ , with  $L$  being the size of the system and  $\zeta$  the roughness exponent. Both  $\beta$  and  $\zeta_{\text{dep}}$  are universal depinning exponents depending on the dimension  $d$  of the interface and on the range  $\alpha$  of the elastic force; but interestingly, not on the disorder

---

<sup>2</sup>See Ref.(36) for a discussion of the correlated disorder case.

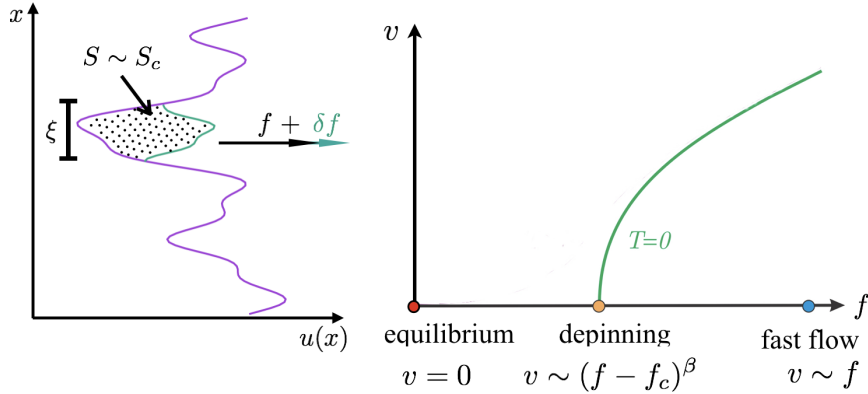


Figure 2: *Left*: Sketch of an avalanche below  $f_c$ : the applied force  $f$  is increased infinitesimally and a finite portion of the interface is destabilized. The size  $S$  of the avalanche corresponds to the spanned area. *Right*: Dynamical phase diagram at zero temperature. At  $f = f_c$  the velocity and the shape of the interface have a universal scaling behavior, the dynamics is characterized by large and scale free avalanches. At  $f = 0$  the interface is in the ground state with a different roughness exponent which depends on the correlation of the disorder (RB or RF). At very large force the interface flows with a velocity that grows linearly with the force and the quenched disorder acts as a thermal noise.

type (20, 46). Slightly above  $f_c$  the dynamics of a point of the interface is highly intermittent: for long times the point is stuck with a vanishing velocity (much smaller than the average value  $v$ ) and suddenly starts to move with a high velocity. In equilibrium second order phase transition the universality arises from the existence of a correlation length that diverges approaching the critical threshold. For depinning the system is out-of-equilibrium but the presence of large spatial correlations is manifested by the collective nature of this intermittent dynamics: at a given time, while many pieces of the interface are at rest, large and spatially connected portions move fast and coherently.

The presence of large correlations can be detected using a quasistatic protocol below (but close to)  $f_c$ . This is shown in **Figure 2 left** where an interface is at rest at a force  $f$ . Upon increasing infinitesimally the force  $f \rightarrow f + \delta f$ , an avalanche takes place: a large portion of the interface advances a finite amount while elsewhere only readjusts infinitesimally ( $\propto \delta f$ ). The avalanches locations cannot be predicted and their sizes (the areas spanned between two consecutive metastable states) present scale free statistics

$$P(S) = S^{-\tau_{\text{dep}}} g(S/S_c) . \quad 4.$$

The Gutenberg-Richter exponent  $\tau$  is universal as are  $\beta$  and  $\zeta_{\text{dep}}$ ,  $g(x)$  is a function that decays fast for  $x \geq 1$  and is constant for  $x < 1$ . The characteristic size of the maximal avalanche increases when  $f \rightarrow f_c^-$ . In practice,  $S_c$  is the clear manifestation of the divergent correlation length  $\xi \simeq |f - f_c|^{-\nu_{\text{dep}}}$  and one expects  $S_c \simeq \xi^{d+\zeta_{\text{dep}}} \simeq |f - f_c|^{-\nu_{\text{dep}}(d+\zeta_{\text{dep}})}$ . Many works have been devoted to describe the dynamics inside an avalanche (47, 33, 34, 28, 48): typically the instability starts well localized at a given point and spreads in space over a distance  $x(t) \simeq t^{1/z}$  up to a time  $t_c \simeq \xi^z$ . For the qEW equation 1 it has been proven that there are only two independent exponents, e.g.  $\zeta_{\text{dep}}$  and  $z$ , and the other can

Table 1: Depinning exponents are known numerically with good precision and saturate to their mean field values for  $d \geq 2\alpha$ . At the depinning RB and RF disorder are in the same universality class. The numerical values of the roughness exponents  $\zeta_{\text{dep}}$  are taken from (49) for  $\alpha = 1$  and from (50) for  $\alpha = 2$ . Those of the dynamical exponent  $z$  are taken from (51) for  $\alpha = 1$   $d = 1$ , from (52) for  $\alpha = 2$   $d = 2$  and from (37) for  $\alpha = 1$   $d = 1$ .

| Depinning exponent   | Observable                               | $d = 1$   | $d = 1$      | $d = 2$      | Mean Field       |
|----------------------|--|---|--------------|--------------|------------------|
|                      |  | $\alpha = 2$  | $\alpha = 1$ | $\alpha = 2$ | $d \geq 2\alpha$ |
| $z$                  | $t(L) \sim L^z$                          | 1.43  | 0.77         | 1.56         | $\alpha$         |
| $\zeta_{\text{dep}}$ | $u(x) \sim x^{\zeta_{\text{dep}}}$       | 1.25  | 0.39         | 0.75         | 0                |
| $\tau_{\text{dep}}$  | $P(S) \sim S^{-\tau_{\text{dep}}}$       | $\tau_{\text{dep}} = 2 - \alpha/(d + \zeta_{\text{dep}})$ |              |              | $3/2$            |
| $\nu_{\text{dep}}$   | $\xi \sim  f - f_c ^{-\nu_{\text{dep}}}$ | $\nu_{\text{dep}} = 1/(\alpha - \zeta_{\text{dep}})$      |              |              | $\alpha^{-1}$    |
| $\beta$              | $v \sim  f - f_c ^\beta$                 | $\beta = \nu_{\text{dep}}(z - \zeta_{\text{dep}})$        |              |              | 1                |

be computed by non trivial scaling relations (see **Table 1**). Note that these relations are valid in low dimensions, because for  $d \geq 2\alpha$  the value of the exponents saturates at their mean field value.

The physics is very different in the limits of very small or very high forces. At  $f = 0$  the interface is at equilibrium in the ground state, its roughness is characterized by a very different (smaller) roughness exponent and the nature of the disorder matters: RF interfaces are rougher than RB. The ground state energy is an extensive quantity (grows as  $L^d$ ) but its sample to sample fluctuations scale as  $L^\theta$ . The energy exponent  $\theta$  obeys the scaling relation  $\theta = 2\zeta_{\text{eq}} + d - \alpha$  (see **Table 2**). This relation is a consequence of the statistical tilt symmetry of the model which assures that the elastic constant  $c$  is not renormalized. On the other hand, assuming that in equilibrium elastic and disorder energy scale in the same way, one has from  $E_{\text{el}}[u] = \frac{c}{2} \int \frac{(u(x',t) - u(x,t))^2}{|x' - x|^{\alpha+d}} d^d x d^d x'$  the relation  $E_{\text{eq}} \propto L^{2\zeta_{\text{eq}}} L^{-(\alpha+d)} L^2 \sim L^{2\zeta_{\text{eq}} + d - \alpha}$ . Note that for  $\alpha > d/2$ , the interface is flat ( $\zeta_{\text{eq}} = 0$ ) and the energy exponent saturates to the central limit value  $\theta = d/2$ .

At  $f \rightarrow \infty$  the quenched pinning reduces to an annealed stochastic noise because in the comoving frame one has  $F_p(x, u) = F_p(x, \delta u + vt) \sim F_p(x, vt)$ . For short-range correlated pinning force, the strength of the disorder plays the role of an effective temperature  $T_{\text{eff}}$ . In this so-called fast-flow regime the motion is not intermittent, and one recovers the standard Edwards Wilkinson dynamics with the generalized fractional laplacian of Eq.2 (53). In particular the dynamical exponent is  $z = \alpha$  and the roughness exponent is  $\zeta_{\text{flow}} = (\alpha - d)/2$  for  $d \leq \alpha$ . For larger dimension, the Edwards Wilkinson interface is flat.

For intermediate forces the physics is not fully governed by any of the three characteristic points described above ( $f = f_c$ ,  $f = 0$  and  $f \rightarrow \infty$ ). Therefore, one could wonder if a completely new scaling description should be introduced. It turns out that it is not the case, at least for  $f > f_c$ . The physics of the interface can be described by a crossover between short length scales, governed by the critical behaviour at  $f = f_c$ , and large length scales, governed by the fixed point of  $f = \infty$ . Below the depinning threshold,  $f < f_c$ , no steady-state can be defined at zero temperature rather than the complete arrest of the interface. The presence of a finite temperature, discussed in the next section, allows to investigate a non-trivial stationary dynamical regime (the creep) with finite velocity at forces in between the equilibrium and the depinning fixed point, and to analyze how this two fixed points affect the dynamics at different scales.

Table 2: Equilibrium exponents for elastic manifold with random bond disorder (RB). For  $\alpha = 2$  the results in  $d = 1$  are exact. In  $d = 2$  we used the numerical results from (54) obtained using a maximal flow algorithm. For  $\alpha = 1$  the results are known from FRG calculations, for RF disorder one expects  $\zeta_{\text{eq}} = \theta = 1/3$ . Note that  $\theta$  and  $\zeta_{\text{eq}}$  are not independent, but obey to the following scaling relation  $\theta = 2\zeta_{\text{eq}} + d - \alpha$ .

| Equilibrium exponent | Observable                        | $d = 1$   | $d = 1$      | $d = 2$       | Mean Field<br>$d \geq 2\alpha$ |
|----------------------|-----------------------------------|---|--------------|---------------|--------------------------------|
|                      |                                   | $\alpha = 2$  | $\alpha = 1$ | $\alpha = 2$  |                                |
| $\theta$             | $E(L) \sim L^\theta$              | 1/3   | $\simeq 0.2$ | $\simeq 0.84$ | $d/2$                          |
| $\zeta_{\text{eq}}$  | $u(x) \sim x^{\zeta_{\text{eq}}}$ | 2/3   | $\simeq 0.2$ | $\simeq 0.41$ | 0                              |
| $\tau_{\text{eq}}$   | $P(S) \sim S^{-\tau_{\text{eq}}}$ | $\tau_{\text{eq}} = 2 - \alpha/(d + \zeta_{\text{eq}})$ |              |               | 3/2                            |
| $\nu_{\text{eq}}$    | $\xi \sim f^{-\nu_{\text{eq}}}$   | $\nu_{\text{eq}} = 1/(\alpha - \zeta_{\text{eq}})$      |              |               | $\alpha^{-1}$                  |

### 2.1. The case of the quenched Kardar-Parisi-Zhang (KPZ) depinning

The quenched Edwards Wilkinson equation and its generalization to long range elasticity are well studied and understood. In all these models the non-stochastic part of the equation is linear in the displacement  $u$  and one can derive the scaling relation of table 1. However, in presence of anisotropies in the disorder (55) or in the elastic interaction (57), a non-linearity becomes relevant for short range elasticity. In this case the equation of motion of the interface writes:

$$\gamma \partial_t u(x, t) = c \nabla^2 u(x, t) + \lambda (\nabla u(x, t))^2 + f + F_p(x, u) . \quad 5.$$

The inclusion of this non-linear term affects the physical behavior as  $f \rightarrow \infty$  leading to the standard Kardar-Parisi-Zhang (KPZ) (58) dynamics rather than the Edwards Wilkinson. At depinning, if  $\lambda f \geq 0$  the motion remains intermittent with large avalanches but with different exponents (59, 56) characterized by new scaling relations, as shown in **Table 3**. When  $\lambda f < 0$  the interface develops a sawtooth shape with an effective exponent  $\zeta_{\text{dep}} = 1$  (60). This regime has been recently observed in (61).

Table 3: Exponents of the qKPZ depinning universality class. The numerical values of the roughness exponent  $\zeta_{\text{dep}}$  are taken from (50). For  $d = 1$  the exponents  $z$  and  $\nu_{\text{dep}}$  are taken from (55), while for  $d = 2$  from (56). The existence of an upper critical dimension is under debate.

| qKPZ exponent        | Observable                               | $d = 1$  | $d = 2$      |
|----------------------|--|--|--------------|
|                      |  | $\alpha = 2$   | $\alpha = 2$ |
| $z$                  | $t(L) \sim L^z$                          | 1  | 1.1          |
| $\zeta_{\text{dep}}$ | $u(x) \sim x^{\zeta_{\text{dep}}}$       | 0.63   | 0.45         |
| $\nu_{\text{dep}}$   | $\xi \sim  f - f_c ^{-\nu_{\text{dep}}}$ | 1.733  | 1.05         |
| $\tau_{\text{dep}}$  | $P(S) \sim S^{-\tau_{\text{dep}}}$       | $\tau_{\text{dep}} = 2 - (\zeta_{\text{dep}} + 1/\nu_{\text{dep}})/(d + \zeta_{\text{dep}})$ |              |
| $\beta$              | $v \sim  f - f_c ^\beta$                 | $\beta = \nu_{\text{dep}}(z - \zeta_{\text{dep}})$   |              |

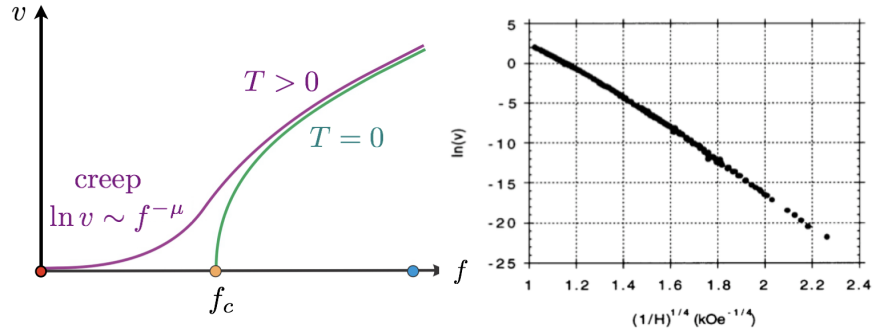


Figure 3: *Left*: Velocity force characteristics at finite temperature. When  $f$  is very small compared to  $f_c$  and at very small temperature, one observes the creep law  $\ln v \sim f^{-\mu}$ . Adapted from (25). *Right*: First experimental verification of a creep law consistent with  $\mu = 1/4$  in 2d ultra-thin Pt/Co/Pt film at room temperature, taken from (62).

### 3. Velocity at finite temperature

At finite temperature the interface has a finite steady velocity  $v$ , even below  $f_c$ . The energy of the interface can be written as the sum of three contributions:

$$E[u] = \int_0^L d^d x \left[ \frac{c}{2} (\nabla u(x))^2 + V_p(x, u(x)) - f u(x) \right], \quad 6.$$

the first term on the RHS being the elastic energy of the interface, the second, the pinning potential, and the third, the energy associated to the driving force  $f$ . We note that the equation of motion (1) is obtained from  $\gamma \partial_t u(x, t) = -\delta E[u]/\delta u(x, t)$ . At finite temperature one can write the associated Langevin equation:

$$\gamma \partial_t u(x, t) = c \nabla^2 u(x, t) + f + F_p(x, u) + \eta(x, t), \quad 7.$$

with  $\langle \eta(x, t) \eta(x', t') \rangle = 2\gamma T \delta(t - t') \delta(x - x')$  where the average is over different realizations of the thermal noise, while the disordered landscape remains fixed.

In presence of a finite drive, the energy Eq. 6 has no lower bound as it is tilted by the force and in average decreases linearly by increasing  $u$ . Yet, the presence of pinning generates metastable states and barriers up to  $f_c$ . The activated motion at finite temperature allows to overcome these barriers yielding a finite steady-state velocity.

The velocity force characteristics is represented in **Figure 3 left**. At very small force and finite temperature a creep regime is observed, where the velocity displays a stretched exponential behavior:

$$v(f, T) = v_0 e^{-\left(\frac{f_T}{f}\right)^\mu}, \quad 8.$$

with  $v_0$  and  $f_T$  depending on the temperature and the microscopic parameters, while  $\mu$  is a universal exponent. This creep law was verified experimentally in ferromagnetic ultrathin films with  $\mu \simeq 1/4$  first by Lemerle *et al.* (62) (see **Figure 3 right**). Rather strikingly, this law can span several decades of velocity (from almost walking speed to nails growth speed) by just varying one decade of the externally applied magnetic field at ambient temperature. The creep law was subsequently found by many other experiments(63, 64) (see Section 6 for a brief review), confirming the universality and robustness of several creep properties. Such universality naturally calls for minimal statistical-physics models on which we will focus.



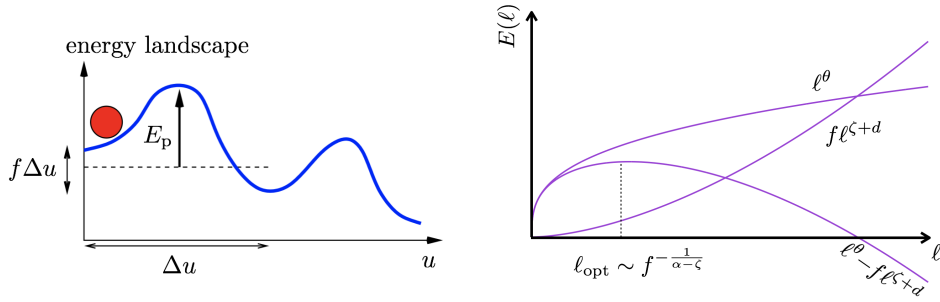


Figure 4: *Left*: Thermally assisted flux flow. The activated velocity of a single degree of freedom in a short range disordered potential is linear in the force and exponentially suppressed by the size of the typical barrier  $E_p$ . *Right*: Creep behavior. The energetic barrier encountered by an interface diverges when the applied force vanishes. Indeed in order to find a new metastable state characterized by smaller energy a large portion of the interface has to reorganize. Scaling arguments predict that the linear size of such reorganization scales as  $\ell_{\text{opt}} \sim f^{-\frac{1}{\alpha-\zeta_{\text{eq}}}}$ .

Eq. 8 has been predicted in (65, 66, 67) and derived within the functional renormalization group technique in (46). The stretched exponential behavior originates from the collective nature of the low temperature dynamics of these extended objects. For a point-like system embedded in a short-range disorder potential the response to a small force will be linear in  $f$ . The idea is to consider that the energy landscape is characterized by valleys at distance  $\Delta u$  separated by an energetic barrier of typical size  $E_p$ . In presence of the tilt introduced by a finite force  $f$ , the energy gap between two consecutive valleys becomes  $\sim f\Delta u$  (see **Figure 4**). According to the Arrhenius law, the time to jump from left to right will be  $e^{\beta(E_p - f\Delta u/2)}$ , while the time for doing it from right to left would be  $e^{\beta(E_p + f\Delta u/2)}$ . Therefore, the velocity can be computed as the thermally assisted flux flow (TAFF (68)) across the barrier:

$$v \propto e^{-\beta(E_p - f\Delta u/2)} - e^{-\beta(E_p + f\Delta u/2)} \simeq e^{-\beta E_p} \Delta u f . \quad 9.$$

We conclude that, in presence of bounded barriers, the velocity will be linear even if with an exponentially suppressed mobility.

For an extended object the typical barrier grows when the external force vanishes and their divergence is at the origin of the stretched exponential behavior in Eq. 8. In **Figure 5** we show different configurations obtained at different times from the direct integration of Eq. 7. At short times one observes incoherent oscillations and the configurations differ only at short length scales. At much larger times the line advances in the direction of the force with a coherent excitation that involves a large reorganization. This collective motion leads the system to a local minimum characterized by a lower energy due to the presence of the force. It is very unlikely that the interface will climb back to the previous configurations characterized by a higher energy. This new and deeper valley is the starting point of a new search in the forward direction. At these time scales the dynamics of the line can be seen as a sequence of metastable states

$$\alpha_1 \rightarrow \alpha_2 \rightarrow \alpha_3 \rightarrow \dots \quad 10.$$

characterized by decreasing energies

$$E_{\alpha_1} > E_{\alpha_2} > E_{\alpha_3} > \dots \quad 11.$$

At low temperature for a given  $\alpha_1, \alpha_2$  is the metastable state with lower energy that can be reached crossing the minimal barrier. It is possible to show that for an interface of internal dimension  $d$  embedded in a  $d + 1$  dimension the pathway obtained with such a rule is the optimal one (and thus the one that dominates the statistics of the dynamics) in the low temperature limit (69).

The first attempts to evaluate the barriers and the length scales associated to this coarse grained dynamics have been done in (65, 66) and in (46) via FRG. The main assumption in their original derivation is that, during the dynamical evolution, the energy barriers scale as the energy fluctuations of the ground state at  $f = 0$ . At equilibrium the fluctuations of the free energy are known to grow with the system size with a characteristic exponent  $\theta$  that depends on the equilibrium roughness exponent via an exact scaling relation  $\theta = 2\zeta_{\text{eq}} + d - \alpha$ . Numerical simulations in (70) have shown that the barriers separating two equilibrium metastable states, that differ on a portion  $\ell$ , grow as  $\ell^\psi$  with an exponent consistent with  $\psi \simeq \theta$ . Using these ideas one can assume that the energy barriers due to the pinning centers and in absence of tilt grow with the size of the reorganization

$$E_p(\ell) \sim \ell^\theta = \ell^{2\zeta_{\text{eq}} + d - \alpha} \quad 12.$$

If the motion is in the forward direction one has to subtract the energy induced by the tilt

$$E_t(\ell) \sim f u(\ell) \ell^d = f \ell^{\zeta_{\text{eq}} + d} \quad 13.$$

In **Figure 4 right** we show that the competition between these two terms (Eqs.12 and 13) yields the characteristic length scale  $\ell_{\text{opt}}$  of the optimal reorganization (and the optimal barrier  $E_p(\ell_{\text{opt}})$ ) allowing to reach a new metastable state with a lower energy:

$$\ell_{\text{opt}} \sim f^{-\frac{1}{\alpha - \zeta_{\text{eq}}}} \quad E_p(\ell_{\text{opt}}) \sim f^{-\frac{\theta}{\alpha - \zeta_{\text{eq}}}}. \quad 14.$$

Using the scaling of  $E_p$  in Eq. 9 one recovers the creep law, Eq. 8, and identifies the creep exponent

$$\mu = \frac{\theta}{\alpha - \zeta_{\text{eq}}} = \frac{2\zeta_{\text{eq}} + d - \alpha}{\alpha - \zeta_{\text{eq}}} \quad 15.$$

as an equilibrium exponent. In particular in  $d = 1$ , for RB disorder and short range elasticity one recovers  $\mu = 1/4$  as in the experiment (62).

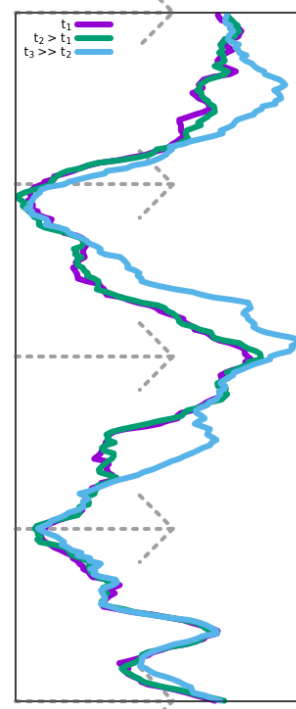


Figure 5: Configurations at different times obtained by direct integration of Eq. 7. At short times one observes incoherent oscillations and the configurations differ only at short length scales. At much larger times the line advances in the direction of the force with a coherent excitation that involves a large reorganization.

Although for the average velocity there is an excellent agreement between the simple scaling arguments (65, 66) and the more sophisticated FRG analysis (46), the FRG showed clearly that other lengthscales besides  $\ell_{\text{opt}}$  (see Figure 4 right) were necessary to describe the motion, pointing to a rich dynamics in the creep regime. In particular the FRG showed that the thermal nucleus led in the dynamics to avalanches at a larger lengthscales than  $\ell_{\text{opt}}$  itself. In order to make a full analysis of the creep regime, a numerical investigation was thus eminently suitable. This is however a highly non-trivial task considering the exponentially large time and length scales. We discuss on how to undertake such a study in the next section.

#### 4. Numerical methods

The direct simulation of the Langevin equation 7 has been performed in (67) and later in (71). This approach confirms a non-linear behavior for the velocity-force characteristics but fails in probing the specific scaling of the creep law. In fact, at low temperature these methods can focus only on the microscopic dynamics describing incoherent and futile oscillations around local minima (see **Figure 5**). The forward motion that allows to escape from these minima occurs at very long time scales that are difficult to reach. In practice one has to increase the temperature or the force bringing the system beyond the validity of the creep scaling hypothesis.

A completely different strategy focus on the coarse grained dynamics at the time scales of the coherent reorganizations that are able to lower the energy. In practice one has to model the interface as a directed polymer of  $L$  monomers at integer positions  $u(i)$ ,  $i = 1, \dots, L$  and with periodic boundary conditions ( $u(L+1) = u(1)$ ). The energy of the polymer is given by:

$$E = \sum_i [(u(i+1) - u(i))^2 - fu(i) + V(i, u(i))]. \quad 16.$$

To reduce the configuration space it is useful to implement a hard metric constraint such that

$$|u(i+1) - u(i)| \leq \kappa, \quad 17.$$

with  $\kappa \sim \mathcal{O}(1)$  an integer.

To model RB disorder one can define  $V_{RB}(i, u) = R_{i,u}$  with  $R_{i,u}$  Gaussian random numbers with zero mean and unit variance, while for RF disorder  $V_{RF}(i, u) = \sum_{k=0}^u R_{i,k}$ , such that  $[\overline{V_{RF}(i, j) - V_{RF}(i', j')}]^2 = \delta_{i,i'} |j - j'|$ .

At the coarse grained level the dynamics corresponds to a sequence of polymer positions determined using a two step algorithm.

- *Thermal activation.* Starting from any metastable state one has to find the compact rearrangement that decreases the energy by crossing the minimal barrier among all possible pathways.
- *Deterministic relaxation.* After the above activated move, the polymer is not necessarily in a new metastable state and relaxes deterministically with the non local Monte Carlo elementary moves introduced in (72).

From the computational point of view the most difficult task is in the first step. In principle, one fixes a maximal barrier and enumerates all possible pathways that stay below the maximal allowed energy. If one of them reaches a state with a lower energy the thermal activation step is over, otherwise the maximal barrier is increased and the process is

repeated. This protocol is exact, it has been implemented in (69), but it has severe computation limitations at low forces as the minimal barrier is expected to diverge for vanishing forces. In order to explore the low force regime, a different strategy has been adopted in (73). Instead of looking to the pathway with the minimal barrier one selects the smallest rearrangement that decreases the energy. This is done by fixing a window  $w$  and computing the optimal path between two generic points  $i, i+w$  of the polymer using the Dijkstra’s algorithm adapted to find the minimal energy polymer between two fixed points. The minimal favorable rearrangement corresponds to the minimal window for which the best path differs from the polymer configuration. Using this strategy, it was possible not only to increase of a factor 30 the system size, but, and more importantly, to decrease of a factor 100 the external drive  $f$ , unveiling the genuine creep dynamics.

### 5. Creep dynamics in the limit of vanishing temperature

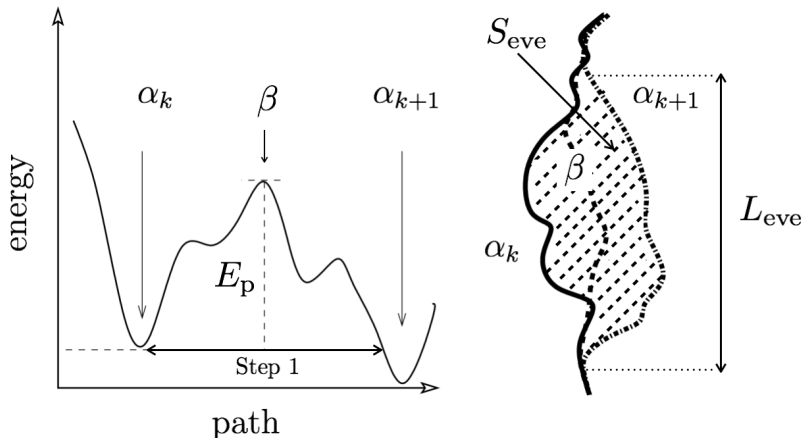


Figure 6: Sketch of the selected pathway starting from the metastable state  $\alpha_k$ . During ‘step one’ of the algorithm one searches for a polymer configuration with an energy smaller than the one associated to  $\alpha_k$  by crossing a minimal barrier  $E_p$ . During ‘step two’ the polymer relaxes deterministically to a metastable configuration, no barriers are overcome at this stage. Adapted from (69).

Here we give a summary of the main results obtained using the coarse grained dynamics introduced in (69, 73). The output of the algorithm is a sequence of metastable states  $\alpha_k$  ( $k = 1, \dots, n$ ), as shown in **Figure 6**. In (69) the barrier  $E_p$  is the minimal between all possible pathways, while in (73) the criterium of the minimal barrier has been approximated with the criterium of the minimal rearrangement which allows to reach much smaller forces and much larger sizes. The area between two subsequent metastable states (see **Figure 6**) defines the size of an activated event. Below this size the dynamics is futile characterized by incoherent vibrations, while once the new metastable state is reached the backward move is suppressed.

### 5.1. Statistics of the events and clusters

From the scaling arguments of Section 3 one expects that the area of the activated events is of the order  $\ell_{\text{opt}}^{d+\zeta_{\text{eq}}}$  with  $\ell_{\text{opt}}$  that grows when the force decreases (see Eq. 14). However the distribution shown in **Figure 7** displays a power law scaling analogous to the depinning one

$$P(S_{\text{eve}}) \sim S_{\text{eve}}^{-\tau} g(S_{\text{eve}}/S_c). \quad 18.$$

When the force decreases the cutoff  $S_c(f)$  grows and displays the scaling predicted in Section 3:

$$S_c \sim \ell_{\text{opt}}^{d+\zeta_{\text{eq}}} \sim f^{-\nu_{\text{eq}}(d+\zeta_{\text{eq}})}. \quad 19.$$

Here  $d = 1$  and  $\zeta_{\text{eq}}$  depends on the nature of the disorder: for RB  $S_c(f) \sim f^{-5/4}$  while for RF  $S_c(f) \sim f^{-2}$ .

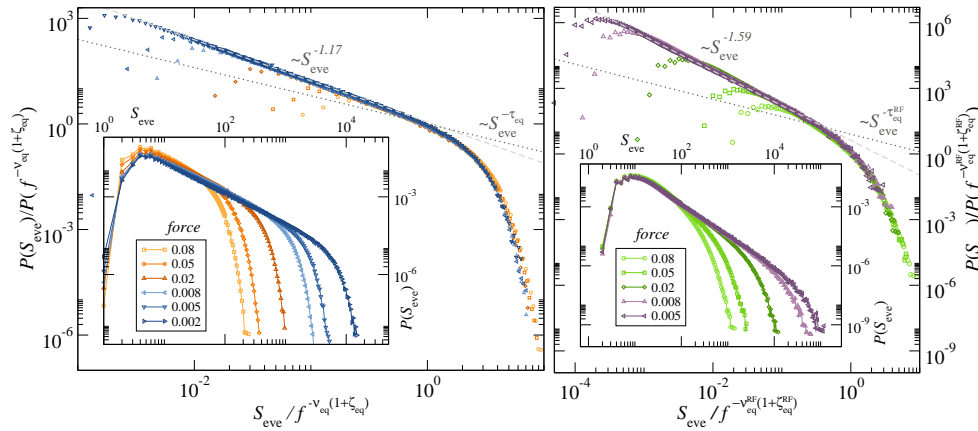


Figure 7: Events size distributions  $P(S_{\text{eve}})$  for RB (*left*) and RF (*right*) at different forces. Main pannels show collapses by plotting  $S_{\text{eve}}/S_c$  with  $S_c(f) = f^{-\nu_{\text{eq}}(1+\zeta_{\text{eq}})}$ . Insets show the unscaled distributions. Note that for RB disorder  $S_c(f) = f^{-5/4}$  while for RF disorder  $S_c(f) = f^{-2}$ . The perfect collapse validates the expected creep scaling  $\ell_{\text{opt}} \sim f^{-\nu_{\text{eq}}}$ , given  $S_c \sim \ell_{\text{opt}}^{(1+\zeta_{\text{eq}})}$ . Adapted from (73).

Eq. 18 implies that the typical activated events are much smaller than the one predicted by scaling arguments. However few very large events dominate the characteristic time scales of the forward motion. The behavior of the velocity in the creep formula is then determined by the occurrence of such large reorganizations. Indeed, the barriers associated to the largest elementary events are expected to scale as  $U_{\text{opt}}(f) \sim \ell_{\text{opt}}^\theta \approx S_c(f)^{\theta/(d+\zeta_{\text{eq}})}$ . Then the mean velocity in the Arrhenius limit writes as  $v \sim \exp[-U_{\text{opt}}/T] \sim \exp[-(f_T/f)^\mu/T]$ , with  $\mu = \theta/(2 - \zeta_{\text{eq}})$ , recovering the celebrated creep law of Eq. 8. The main difference with the previous scaling approaches (65, 66) is that the creep law is not determined by the ‘typical’ events but by the largest ones instead.

To get further inside on the sequence of these events one notes that the exponent  $\tau$  of  $P(S_{\text{eve}})$  is larger than the one expected in equilibrium (in particular in **Figure 7** for RB  $\tau = 1.17$  instead of  $\tau_{\text{eq}} = 4/5$  and for RF  $\tau = 1.59$  instead of  $\tau_{\text{eq}} = 1$ ). The anomaly observed in the exponent  $\tau$  is the first fingerprint of a discrepancy between creep events distributions and other type of avalanches, as the depinning ones, going well beyond the

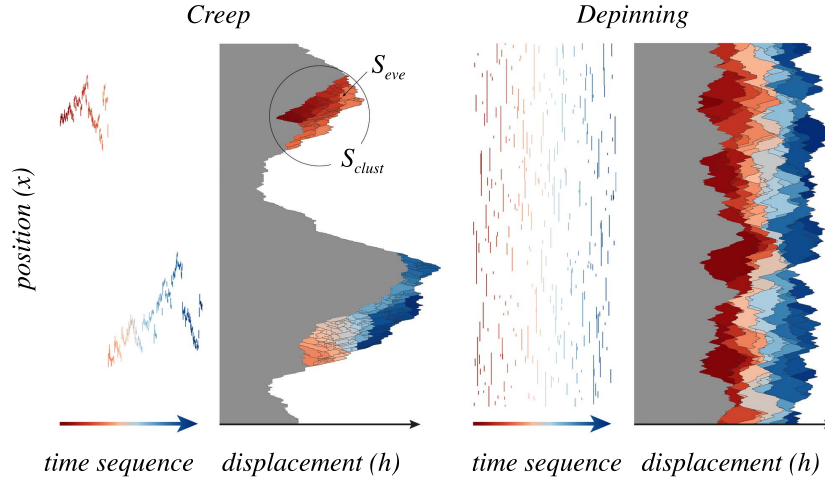


Figure 8: *Left*: Sequence of activated events in the creep regime. First, in the activity map, each segment corresponds to an event and displays its longitudinal length. The full configurations of 300 consecutive metastable states are shown immediately after. An individual event of size  $S_{eve}$  and a cluster of size  $S_{clust}$  are exemplified. *Right*: Sequence of deterministic avalanches close to the depinning that appear randomly distributed in space. Again, both activity map and sequence of configurations are shown. Adapted from (73).

anticipated differences of critical exponents. In **Figure 8** it is shown that the typical sequence of avalanches is randomly located in space while the creep events are organized in spatio-temporal patterns very similar to earthquakes: the large events are the main shocks that are followed by a cascade of small activated events. The events in the cascade are the analogous of the aftershocks which are responsible of an excess of small events in the Gutenberg-Richter exponent as reported also in the analysis of the real earthquakes (31, 74, 33)<sup>3</sup>. Similar patterns for the elementary activated were observed below but near the depinning threshold (75).

In order to analyze the spatio-temporal patterns one can study the clusters of correlated events, defined by the activated events enclosed by a circle in **Figure 8**. All details in the definition of the clusters are found in (73).

Surprisingly, for both RB and RF disorder, the statistics of the clusters appear as the one of the depinning avalanches with  $\tau_{dep} = 1.11$  and the cut-off controlled by the system size and diverging in the thermodynamic limit (76) (see **Figure 9**).

## 5.2. Geometry of the interface

An independent and complementary confirmation of these results comes from the study of the roughness of the interface at different scales as introduced in (69). In practice one measures the structure factor  $S(q) = \overline{u(q)u(-q)} \sim q^{-(d+2\zeta)}$  where  $u(q)$  is the Fourier

<sup>3</sup>The Gutenberg-Richter exponent  $b = \frac{3}{2}(\tau-1)$  for the earthquake magnitude distribution should be smaller than the mean field prediction  $\frac{3}{4}$ , but from seismic records one gets (33, 31)  $b \simeq 1$

transform of the position of the interface and the overline represents the average over many configurations. The insets of **Figure 9** shows that there exists a crossover  $1/q_c \sim \ell_{\text{opt}}$  between two different behavior of the roughness: at small length scales the interface seems to be at equilibrium, while at large length scales it appears at depinning. This observation supports the idea that the clusters are depinning-like above a scale  $\ell_{\text{opt}}$ . Although such a result is consistent with the predictions obtained by FRG in (46), it should be stressed that these clusters with depinning statistics above  $\ell_{\text{opt}}$  are formed by several *activated* events rather than generated by a single deterministic move.

The coarse grained dynamics studied here is in the limit of vanishing temperature. At finite temperature the velocity is non-zero and this induces that the fast flow roughness becomes relevant at the large length scales (see **Figure 10**). The crossover occurs at a scale  $\xi$  that diverges at vanishing temperature. The FRG proposes a scaling form for  $\xi$  at low temperature and force which depends on  $f$  and  $T$  (46), but this form was never tested in numerical simulation or experiments.

**Quenched Edwards-Wilkinson (qEW) to quenched KPZ (qKPZ) crossover.** The roughness exponent measured at large scales  $\zeta_{\text{dep}} \approx 1.25$  (see the inset of **Figure 9**) is in agreement with the depinning exponent of the quenched Edwards-Wilkinson universality class.

The qEW depinning exponents are expected when the elastic interactions are harmonic and short range as in Eq. 6. When the interactions are anharmonic (57, 77) or a metric constraint as Eq. 17 is present, the depinning is in the quenched KPZ universality class. In particular the roughness exponent is expected to be  $\zeta_{\text{dep}}^{\text{qKPZ}} \approx 0.63$  (57, 69). The reasons of why simulations deep in the creep regime (but with the metric constraint of (17)) apparently display a crossover from  $\zeta_{\text{eq}}$  to  $\zeta_{\text{dep}}$  instead of a crossover from  $\zeta_{\text{eq}}$  to  $\zeta_{\text{dep}}^{\text{qKPZ}}$  are analyzed in (78). The exponents of the qEW universality class show up at an intermediate regime, but

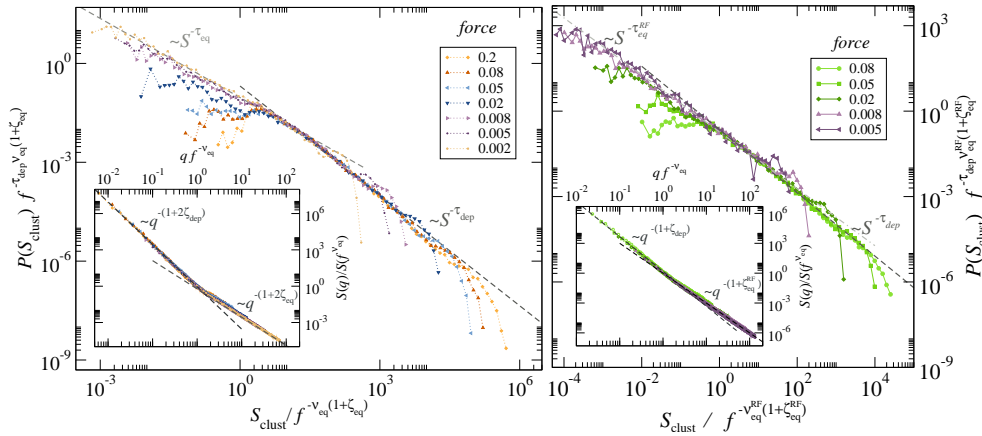


Figure 9: Cluster area distribution  $P(S_{\text{clus}})$  for different forces for RB (*left*) and RF (*right*) disorder. A characteristic size  $S_c(f)$  separates small clusters that follow *equilibrium*-like statistics from big clusters that follow a *depinning*-like one. This result is confirmed by the study of the rescaled structure factor  $S(q)$  for the same forces (insets): a geometrical crossover is observed from *equilibrium*-like roughness at small scales to a *depinning*-like roughness at large scales. Adapted from (73).

at very large scales the qKPZ exponents are recovered, as expected. The crossover between the two depinning regimes is estimated to be

$$L_{\text{anh}} \propto \ell_{\text{opt}}^{\frac{\zeta_{\text{dep}} - \zeta_{\text{eq}}}{\zeta_{\text{dep}} - 1}}. \quad 20.$$

For small forces the crossover occurs at very large sizes and it cannot be observed numerically. However, at larger forces the crossover can be observed as shown in **Figure 11 left** for the structure factor and in **Figure 11 right** for the cluster size statistics.

### 5.3. Optimal Paths and Barriers

The exact algorithm for simulating the coarse-grained dynamics below the depinning threshold is computationally expensive but has the advantage that gives access to the energy barriers of the activated motion (69). If the interface moves on a torus (namely, periodic boundary conditions are assumed both in  $x$  and in  $u$ ) the dynamics reaches a stationary state independent on the initial condition, with a finite sequence of metastable states  $\alpha_k$  separated by barriers  $E_p(\alpha_k \rightarrow \alpha_{k+1})$  that can be computed exactly.

Barriers are important, since the Arrhenius activation formula tell us that at vanishing temperatures the steady state forward motion of the elastic interface is fully controlled in a finite sample by the largest barrier  $U = \max_k E_p(\alpha_k \rightarrow \alpha_{k+1})$  encountered in the stationary sequence of metastable states. The dominant configuration  $\alpha_{k^*}$  such that  $U = E_p(\alpha_{k^*} \rightarrow \alpha_{k^*+1})$  is the largest barrier in a given sample plays a role similar to a ground state configuration in an equilibrium system; in the sense that its attributes tend to dominate the average properties at low enough temperatures (compared with the gap between the first and second largest energy barriers).

In **Figure 12 left** we show the mean value  $\bar{U}$  as a function of the force. As expected from the creep formula  $\bar{U}$  grows with decreasing the force. Unfortunately, the computational cost of applying the exact algorithm is too high to verify the asymptotic scaling  $\bar{U} \sim f^{-\mu}$  when  $f \rightarrow 0$ . When  $f \rightarrow f_c$ , the barrier vanishes and the size of the activated event

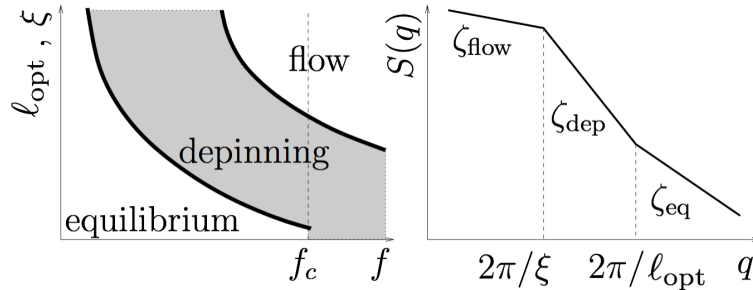


Figure 10: *Left*: Dynamical phase diagram proposed in (46) at finite temperature. Below  $f_c$  the crossover between equilibrium and depinning occurs at the scale  $\ell_{\text{opt}}$ . At finite temperature there is also a crossover at a length scale  $\xi$  between depinning and fast flow. However  $\xi$  diverges in the limit of small temperature. *Right*: Behavior of the roughness measured from the structure factor consistent with the dynamical phase diagram. Adapted from (69).



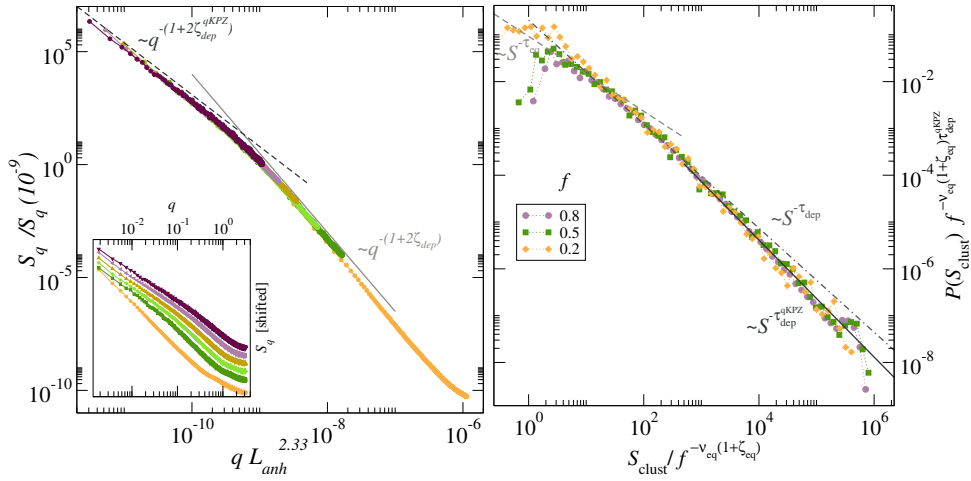


Figure 11: *Left*: Structure factor for the Random Bond case showing the characteristic lengthscale  $L_{\text{anh}}$  which separate the harmonic depinning regime with roughness exponent  $\zeta_{\text{dep}}$  from the anharmonic depinning regime with exponent  $\zeta_{\text{dep}}^{\text{qKPZ}}$ , for different high forces  $f \in \{0.2, 0.5, 0.6, 0.7, 0.8, 0.9\}$ ,  $L = 3360$ . The bottom-left inset shows the raw structure factor arbitrarily shifted in the vertical direction for different forces for a better display. The main panel shows the structure factor rescaled with  $L_{\text{anh}} \propto (\ell_{\text{opt}}/L_c)^{7/3}$ , as proposed in Eq. 20 for RB disorder. Straight gray lines are a guide to the eye, showing slopes corresponding to  $\zeta_{\text{dep}} \simeq 1.25$  (full line) and  $\zeta_{\text{dep}}^{\text{qKPZ}} \simeq 0.65$  (dash line). *Right*: Cluster size distributions for  $L = 3360$  and  $f \in \{0.2, 0.5, 0.8\}$ . The anharmonic crossover has consequences in the cluster distribution for large cluster sizes. In the depinning regime the power law decay has a crossover from a regime described by  $\tau_{\text{dep}} \simeq 1.11$  to a regime described by  $\tau_{\text{dep}}^{\text{qKPZ}} \simeq 1.25$  indicated by the two dashed lines. Adapted from (78).

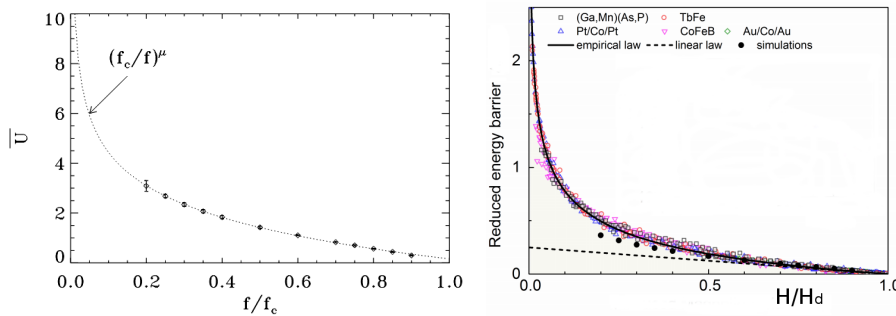


Figure 12: *Left*: Average over disorder realizations of the dominant barrier, as obtained by using the exact transition pathways algorithm. Adapted from (69). *Right*: Rescaled energy barrier as a function of  $H/H_{\text{dep}}$  for different materials and temperatures ranging from 10 to 315 K (25 curves in total), from (79). Black circles correspond to the barriers shown on the left.

becomes of the order of the Larkin length, the length for which the relative displacements

are of the order of the interface thickness (or the correlation length of the disorder) (24). This matches nicely with the behavior expected for the critical configuration at  $f = f_c$ . There, the barrier is zero as the configuration is marginally stable and the soft mode is localized (Anderson-like) with a localization length that can be identified with the Larkin length (80). In **Figure 12 right** we show the same quantity obtained in experiments for different ferromagnetic domain walls.

## 6. Comparison with Experiments

The creep regime has been studied in different types of domain walls. Paradigmatic examples are domain walls in thin film ferromagnets with out of plane anisotropy (12), driven by an external magnetic field or by an external electric current. In these systems, the domain walls can be directly observed by microscopy techniques based on magneto-optic Kerr effect (MOKE). This allows to measure the mean velocity as a function of the applied field and the domain wall geometry. More recently, the analysis of the images has allowed to identify the sequence of events connecting different metastable domain wall configurations in presence of a uniform weak drive. In this section we briefly review part of such experimental literature. For a dedicated review of the experimental literature on magnetic domain walls up to 2013, including reports of different values of  $\mu$  and strong pinning issues, see (12). As a side remark we also mention the possibility to study the creep regime of domain walls in ferroelectric materials driven by an external electric field and observed with piezoforce microscopy (14, 15).

### 6.1. Creep Velocity

The creep law Eq. 8 was first experimentally tested in thin ferromagnetic films (Pt/Co(0.5nm)/Pt) driven by a magnetic field  $H$  by Lemerle *et al.* (62). They observed a clear stretched exponential behavior ( $\log v \propto -H^{-\mu}$ ) of the stationary mean velocity as a function of the applied field. Rather strikingly, such law can span several decades of velocity, from almost walking speeds to the speed of nails growth. The creep exponent  $\mu$  was found to be compatible with the prediction  $\mu = (2\zeta_{\text{eq}} - 1)/(2 - \zeta_{\text{eq}}) = 1/4$  where the equilibrium roughness  $\zeta_{\text{eq}} = 2/3$  corresponds to a RB disorder. A confirmation of the validity of the creep predictions was reported later in a study of Ta/Pt/Co<sub>90</sub>Fe<sub>10</sub>(0.3nm)/Pt ferromagnetic thin film wires (63). In this paper not only Eq. 8 with  $\mu \approx 1/4$  was verified, but it was also observed a dimensional crossover ( $d : 1 \rightarrow 0$ ) in the velocity force characteristic at low field. Indeed, decreasing the magnetic field the length scale  $\ell_{\text{opt}}$  grows as  $\sim H^{-\nu_{\text{eq}}}$  with  $\nu_{\text{eq}} = 1/(2 - \zeta_{\text{eq}})$  up to the size of the wire's width where it saturates. As a consequence the barrier  $E_p \sim \ell_{\text{opt}}^\theta$  saturates inducing the breakdown of the creep law of Eq. 8 when  $\ell_{\text{opt}}$  becomes of the order of the wire width. A dimensional crossover ( $d : 1 \rightarrow 0$ ) then takes place, from creep, Eq. 8, to a TAFF like regime, Eq. 9.

From the creep theory perspective the experiments of Refs. (62, 63) hence provide crucial information: (i) Although domain walls are actually two dimensional objects in three dimensional materials, they effectively behave as a simpler one dimensional elastic object. In other words, the thickness of the magnetic film is smaller than  $\ell_{\text{opt}}$  and the dynamics is governed by energy barriers with  $\theta(d = 1)$ . (ii) Dipolar interactions originated by stray magnetic fields seem to be unimportant otherwise the nonlocal elasticity would change the exponent  $\mu$ . (iii) The disorder is of RB type as for RF disorder one expects

$\zeta_{\text{eq}} = 1$ , yielding  $\mu = 1$ . This is particularly relevant, since the nature of the DW pinning is one of the less controlled properties of the hosting materials.

In particular since the pioneer work by Lemerle *et al.* (62) there have been several recent works in thin magnetic systems reporting a consistent creep behavior with a mean domain wall velocity showing a stretched exponential law with  $\mu = 1/4$  at low enough driving fields (12, 79, 64, 81, 82, 83, 84, 85, 86, 87) and for different temperatures (79). The energy barrier encountered by the wall has been estimated using the Arrhenius formula  $U = -K_B T \log v/v_0$  with  $v_0$  is a characteristic field independent velocity (64). Its behavior as a function of  $H$  was found to be universal for a large family of materials:  $U$  diverges at small fields as predicted by the creep law,  $U \sim H^{-\mu}$  and vanishes at the depinning field as  $U \sim (H - H_d)$  (see **Figure 12 right**). Both asymptotic behaviors are well described by the matching expression  $U \sim (1 - (H_d/H)^\mu)$ . Moreover, the behavior experimentally observed for  $U$  as a function of  $H$  is in perfect agreement with the value  $\bar{U}$  found in (69) and shown in **Figure 12 left**.

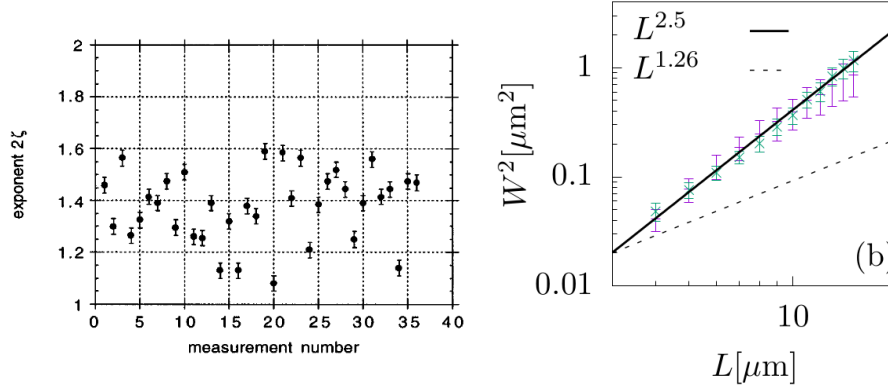


Figure 13: *Left*: Roughness exponents obtained in (62) by fitting the displacement correlator function  $\overline{[u(x+L) - u(x)]^2} \sim L^{2\zeta}$  with  $1\mu\text{m} < L < 15\mu\text{m}$  and  $v = 7\text{nm/s}$ . The average exponent is  $\zeta \approx 0.69 \pm 0.07$ . *Right*: Roughness exponent obtained in (84) by fitting the detrended width. Different symbols correspond to two domain wall configurations at  $v \approx 2\text{nm/s}$ . The solid line indicates a qEW scaling  $2\zeta_{\text{dep}} \approx 2.5$ , the dashed line a qKPZ scaling  $2\zeta_{\text{dep}}^{\text{qKPZ}} = 1.26$ .

## 6.2. The Roughness puzzle

Another important test of the creep theory is to study the steady-state roughness of the interface. From **Figure 10** we expect that the width of a domain wall of size  $L$ ,  $w(L)$  (see Eq. 3) should scale as

$$w^2(L) \sim \begin{cases} L^{2\zeta_{\text{eq}}} & \text{if } L < \ell_{\text{opt}} \\ L^{2\zeta_{\text{dep}}} & \text{if } \ell_{\text{opt}} < L < \xi \\ L^{2\zeta_{\text{flow}}} & \text{if } \xi < L. \end{cases} \quad 21.$$

Lemerle *et al.* (62) and various following works report  $\zeta \approx 0.7 \pm 0.1$ , in agreement with the equilibrium value  $\zeta_{\text{eq}} = 2/3$  but far from the depinning qEW universality class  $\zeta_{\text{dep}} = 1.25$ .

As we discuss below however, in the light of the current theory for creep and more recent experiments, the identification of the observed  $\zeta$  with  $\zeta_{\text{eq}} = 2/3$  can not be justified, calling for a new reinterpretation of the data.

Recently, Gorchon et al. (79) studied field-driven domain walls in the prototypical ultrathin Pt/Co(0.45nm)/Pt ferromagnetic films. By fitting the velocity force characteristics in the creep and depinning regimes, they determined the critical depinning field  $H_{\text{dep}} \approx 1000$  Oe and a characteristic energy scale  $T_{\text{dep}} \approx 2000$  K at room temperature ( $T = 300$  K). With these values it is possible to estimate  $\ell_{\text{opt}}$  using the assumptions of weak pinning (88, 89, 90):

$$\ell_{\text{opt}} = L_c (H_{\text{dep}}/H)^{\nu_{\text{eq}}} \tag{22}$$

$$L_c = (k_B T_{\text{dep}})/(M_s H_{\text{dep}} w_c \delta)$$

The microscopic Larkin length  $L_c$  can be evaluated as a function of the domain wall width  $w_c$ , the thickness of the sample  $\delta$  and the saturation magnetization  $M_s$ . All these micromagnetic parameters are known, yielding  $L_c \approx 0.04 \mu\text{m}$  (see (83) for the analysis for different materials). Using a spatial resolution of  $1 \mu\text{m}$ , typical for MOKE setups and the measured  $H_{\text{dep}} \approx 1000$  Oe one can get the condition  $H \lesssim 0.4$  Oe at room temperature to resolve the typical thermal nucleus size, i.e.  $\ell_{\text{opt}} > 1 \mu\text{m}$ . Interestingly,  $\ell_{\text{opt}}$  was estimated in Ta/Pt/Co<sub>90</sub>Fe<sub>10</sub>(0.3nm)/Pt wires (63) with a completely different method, observing finite size effects as the wire width  $w$  was reduced. A good scaling  $\ell_{\text{opt}} \sim H^{-\nu_{\text{eq}}}$  with 1- $d$  RB exponents, compatible with  $\zeta_{\text{eq}} = 2/3$ , was found. For these samples a field of  $H = 16$  Oe gives  $\ell_{\text{opt}} \approx 0.16 \mu\text{m}$ , remarkably in good agreement with the above estimate for the Pt/Co/Pt film. Unfortunately, no direct roughness exponent measurements were reported in Ref (63). The above estimates suggest that the range of length scales used to fit experimentally the roughness exponent exceed the size of  $\ell_{\text{opt}}$ . This implies that the value  $\zeta \sim 0.6 - 0.7$  recorded in (62, 91, 92, 86, 93) can not be interpreted as an equilibrium exponent and must actually correspond to the depinning regime or to the fast flow regime of roughness (see **Figure 2**)

The fast flow exponent predicted for RB or RF systems is  $\zeta_{\text{flow}} = 1/2$  both for RB or RF systems, quite far from the observed values. For short range elasticity there are two universality classes at the depinning transition: the qEW with a roughness exponent  $\zeta_{\text{dep}} \simeq 1.25$  and the quenched KPZ with  $\zeta_{\text{dep}}^{\text{qKPZ}} \simeq 0.63$ . The first value is consistent with the roughness exponent obtained in (84) at low velocity, while the last value is remarkably close to the values at higher velocity reported in (62). A possible way to solve this puzzle is to invoke a crossover qEW / quenched KPZ already observed in the numerical simulations in Section 5.2. There, at low drive, the crossover occurs at very large length scales, and the qEW exponents are measured. At higher drive the quenched KPZ is recovered already at short distances. To invoke such an identification however, we have to justify the presence of a KPZ term in the effective DW equation of motion. At least two mechanisms can justify the presence of a non-linear KPZ term: (i) A kinetic mechanism yields  $\lambda \sim v$  (58) for interfaces driven by a pressure (i.e. driven by a force locally normal to the interface). (ii) A quenched disorder mechanism induced by the anisotropy of the disorder (55) or anharmonicities in the elasticity (57, 50, 77) yields a velocity independent  $\lambda$ . At the depinning transition only the second mechanism is relevant but at the moment we lack a microscopic derivation and the presence of crossovers between qEW and qKPZ is still under debate.

To shed light on this puzzle another important ingredient that should potentially be

taken into account is the presence of defects such as bubbles and overhangs, at short length-scales. The effects of these defects on the large scale properties of the domain wall are not yet well understood. Large scale simulations on the 3-*d* random field Ising model showed an anomalous behavior of the roughness of the interface which doesn't match with the qEW prediction (94) (see also (95)).

### 6.3. Creep avalanches

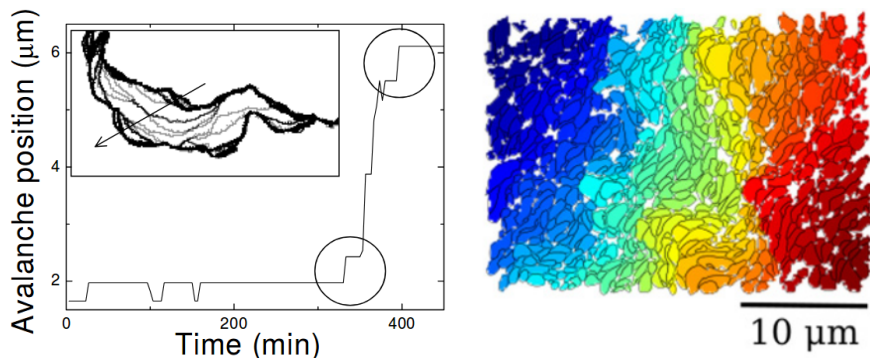


Figure 14: *Left*: Large reorganizations as obtained by Repain *et al.* (96) in irradiated Pt/Co/Pt thin films. The inset shows the successive domain wall configurations in a  $92 \times 28 \mu\text{m}^2$  field of view. Time interval between two images is  $\Delta t = 200$  s. *Right*: Sequences of magnetization reversal areas detected deep in the creep regime of Pt/Co/Pt thin films, as obtained by Grassi *et al.* (84). In this image time windows of  $\Delta t = 15$  s were used.

A direct experimental access to the thermal activated events and clusters would constitute a strong test for the current theoretical picture.

Repain *et al.* in (96) observed reorganizations in the creep regime whose characteristic size qualitatively increases when lowering the field. It is not clear if these reorganizations can be identified with the thermal activated events as they look like chains of concatenated arcs (see inset in Fig.14) suggesting the presence of strong diluted pinning. More recently, Grassi *et al.* (84) performed a detailed and more quantitative analysis in non-irradiated Pt/Co/Pt films, focusing on regions of the sample where strong pinning was not present. They observed almost independent thermally activated reorganizations. Their observations are consistent with the existence of “creep avalanches” with broad size and waiting-time distributions. It is tempting to identify them with the clusters found in numerical simulations discussed in Section 5.1.

The quantitative experimental study of creep events remains a big experimental challenge. The single thermally activated event or “elementary creep event” of Sec 5 appears to be systematically too small to be resolved by Kerr microscopy, even for velocities of order of  $v \sim 1$  nm/s. Partially developed clusters appear to be accessible however, yielding indirect information about the elementary events that control the mean creep velocity. Understanding the effect of strong diluted pinning mixed with weak dense pinning is of crucial importance for a quantitative analysis, since elementary activated events could be equally associated to the collective rearrangements of typical size  $\ell_{\text{opt}}$  or to activated depinning from strong centers.

## 7. Conclusions and Perspectives

Elastic interfaces driven in disordered media represent a dramatic simplification of physical systems, such as magnetic domain walls in disordered ferromagnets. However, by encompassing the key interplay between elasticity and disorder, these models are able to predict with extraordinary precision some properties which are practically impossible to infer from more realistic microscopic approaches. An important example is provided by the creep regime. The theoretical picture is now well understood:

- The velocity versus the force characteristics displays a stretched exponential behavior.
- The geometrical properties of the interface show a crossover from an equilibrium-like behavior at short length scales to a depinning-like behavior at large length scales.
- The dynamics displays spatio-temporal patterns (“creep avalanches”) made of many correlated activated events. The statistical properties of these avalanches are described by the depinning critical point.

The creep regime is relevant for many physical systems, ranging from fracture fronts, contact lines or ferroelectric domain walls. The most striking confirmation comes however from the experiments in ferromagnetic films. There, the stretched exponential behavior of the velocity is today well established. More recently, the analysis of the MOKE images showed the fingerprints of an avalanche creep dynamics.

Despite of the success of the elastic interface model many important questions remain open. First, the statistical properties of the creep avalanches are still an experimental challenge: the elementary events are too small to be resolved with MOKE microscopy and the spatio-temporal correlations have not been characterized. Second, there is a mismatch between the roughness exponents observed in numerical simulations and the ones observed experimentally. To find a solution for this puzzle is probably one of the biggest current challenges in the field. We hope these questions will motivate further research on the universal collective dynamics of elastic interfaces in random media.

## DISCLOSURE STATEMENT

The authors are not aware of any affiliations, memberships, funding, or financial holdings that might be perceived as affecting the objectivity of this review.

## ACKNOWLEDGMENTS

We warmly acknowledge collaborations and uncountable vivid discussions with E. Agoritsas, S. Bustingorry, J. Curiale, G. Durin, E. A. Jagla, V. Jeudy, W. Krauth, V. Lecomte, P. Le Doussal, P. Paruch and K. Wiese. We acknowledge the France-Argentina project ECOS-Sud No. A16E01. ABK acknowledges partial support from grants PICT2016-0069/FONCyT from Argentina. EEF acknowledges support from grant PICT 2017-1202, ANPCyT (Argentina). TG support from the Swiss National Science foundation under Division II. This work is supported by “Investissements d’Avenir” LabEx PALM (ANR-10-LABX-0039-PALM) (EquiDystant project, L. Foini).

## LITERATURE CITED

1. Eds: Barrat JL, Dalibard J, Feigelman M, Kurchan J. 2003. Slow relaxations and nonequilibrium dynamics in condensed matter. Springer, Berlin
2. Berthier L, Biroli G. 2011. *Reviews of Modern Physics* 83:587
3. Anderson PW. 1958. *Physical review* 109:1492
4. Evers F, Mirlin AD. 2008. *Reviews of Modern Physics* 80:1355
5. Sethna JP, Dahmen KA, Myers CR. 2001. *Nature* 410:242
6. Baret JC, Vandembroucq D, Roux S. 2002. *Physical review letters* 89:195506
7. Lin J, Lerner E, Rosso A, Wyart M. 2014. *Proceedings of the National Academy of Sciences* 111:14382–14387
8. Nicolas A, Ferrero EE, Martens K, Barrat JL. 2018. *Reviews of Modern Physics* 90:045006
9. Bonamy D, Bouchaud E. 2011. *Physics Reports* 498:1–44
10. Schmittbuhl J, Roux S, Vilotte JP, Måløy KJ. 1995. *Physical Review Letters* 74:1787
11. Bonamy D, Santucci S, Ponson L. 2008. *Physical review letters* 101:045501
12. Ferré J, Metaxas PJ, Mougin A, Jamet JP, Gorchon J, Jeudy V. 2013. *Comptes Rendus Physique* 14:651 – 666. Disordered systems / Systèmes désordonnés
13. Zapperi S, Cizeau P, Durin G, Stanley HE. 1998. *Physical Review B* 58:6353
14. Paruch P, Guyonnet J. 2013. *Comptes Rendus Physique* 14:667–684
15. Kleemann W. 2007. *Annu. Rev. Mater. Res.* 37:415–448
16. Moulinet S, Rosso A, Krauth W, Rolley E. 2004. *Physical Review E* 69:035103
17. Le Doussal P, Wiese KJ, Moulinet S, Rolley E. 2009. *EPL (Europhysics Letters)* 87:56001
18. Dhar D. 1999. *Physica A: Statistical Mechanics and its Applications* 263:4–25
19. Henkel M, Hinrichsen H, Lübeck S, Pleimling M. 2008. Non-equilibrium phase transitions. vol. 1. Springer
20. Narayan O, Fisher DS. 1993. *Phys. Rev. B* 48:7030–7042
21. Thomas Nattermann, Semjon Stepanow, Lei-Han Tang, Heiko Leschhorn. 1992. *J. Phys. II France* 2:1483–1488
22. Fisher DS. 1998. *Physics Reports* 301:113–150
23. Müller M, Gorokhov DA, Blatter G. 2001. *Phys. Rev. B* 63:184305
24. Agoritsas E, Lecomte V, Giamarchi T. 2012. *Physica B: Condensed Matter* 407:1725 – 1733. Proceedings of the International Workshop on Electronic Crystals (ECRYS-2011)
25. Ferrero EE, Bustingorry S, Kolton AB, Rosso A. 2013. *Comptes Rendus Physique* 14:641 – 650. Disordered systems / Systèmes désordonnés
26. Kardar M. 1998. *Physics Reports* 301:85–112
27. Rosso A, Le Doussal P, Wiese KJ. 2009. *Physical Review B* 80:144204
28. Kolton AB, Doussal PL, Wiese KJ. 2019. *EPL (Europhysics Letters)* 127:46001
29. Papanikolaou S, Bohn F, Sommer RL, Durin G, Zapperi S, Sethna JP. 2011. *Nature Physics* 7:316
30. Laurson L, Illa X, Santucci S, Tallakstad KT, Måløy KJ, Alava MJ. 2013. *Nature communications* 4:2927
31. Scholz CH. 2002. The mechanics of earthquakes and faulting. Cambridge university press
32. Jagla E, Kolton A. 2010. *Journal of Geophysical Research: Solid Earth* 115
33. Jagla EA, Landes FP, Rosso A. 2014. *Phys. Rev. Lett.* 112:174301
34. Janičević S, Laurson L, Måløy KJ, Santucci S, Alava MJ. 2016. *Physical review letters* 117:230601
35. Kolton AB, Rosso A, Giamarchi T, Krauth W. 2006. *Phys. Rev. Lett.* 97:057001
36. Fedorenko AA, Le Doussal P, Wiese KJ. 2006. *Phys. Rev. E* 74:061109
37. Ferrero EE, Bustingorry S, Kolton AB. 2013. *Phys. Rev. E* 87:032122
38. Narayan O, Fisher DS. 1992. *Phys. Rev. B* 46:11520–11549
39. Le Doussal P, Wiese KJ, Chauve P. 2002. *Phys. Rev. B* 66:174201
40. Fisher DS. 1985. *Phys. Rev. B* 31:1396–1427

41. Alessandro B, Beatrice C, Bertotti G, Montorsi A. 1990. *Journal of Applied Physics* 68:2908–2915
42. Doussal PL, Vinokur VM. 1995. *Physica C: Superconductivity* 254:63 – 68
43. Joanny J, De Gennes PG. 1984. *The journal of chemical physics* 81:552–562
44. Gao H, Rice JR. 1989. *Journal of applied mechanics* 56:828–836
45. Kolton AB, Jagla EA. 2018. *Phys. Rev. E* 98:042111
46. Chauve P, Giamarchi T, Le Doussal P. 2000. *Phys. Rev. B* 62:6241–6267
47. Le Doussal P, Wiese KJ. 2013. *Phys. Rev. E* 88:022106
48. Priol CL, Doussal PL, Ponson L, Rosso A. 2019. *arXiv preprint arXiv:1909.09075*
49. Rosso A, Krauth W. 2002. *Phys. Rev. E* 65:025101
50. Rosso A, Hartmann AK, Krauth W. 2003. *Phys. Rev. E* 67:021602
51. Ramanathan S, Fisher DS. 1998. *Phys. Rev. B* 58:6026–6046
52. Leschhorn H. 1993. *Physica A: Statistical Mechanics and its Applications* 195:324 – 335
53. Zoia A, Rosso A, Kardar M. 2007. *Phys. Rev. E* 76:021116
54. Middleton AA. 1995. *Phys. Rev. E* 52:R3337–R3340
55. Tang LH, Kardar M, Dhar D. 1995. *Phys. Rev. Lett.* 74:920–923
56. Buldyrev SV, Havlin S, Stanley HE. 1993. *Physica A: Statistical Mechanics and its Applications* 200:200–211
57. Rosso A, Krauth W. 2001. *Phys. Rev. Lett.* 87:187002
58. Kardar M, Parisi G, Zhang YC. 1986. *Physical Review Letters* 56:889
59. Tang LH, Leschhorn H. 1992. *Phys. Rev. A* 45:R8309–R8312
60. Jeong H, Kahng B, Kim D. 1996. *Phys. Rev. Lett.* 77:5094–5097
61. Atis S, Dubey AK, Salin D, Talon L, Le Doussal P, Wiese KJ. 2015. *Phys. Rev. Lett.* 114:234502
62. Lemerle S, Ferré J, Chappert C, Mathet V, Giamarchi T, Le Doussal P. 1998. *Phys. Rev. Lett.* 80:849–852
63. Kim KJ, Lee JC, Ahn SM, Lee KS, Lee CW, et al. 2009. *Nature* 458:740 EP –
64. Jeudy V, Mougín A, Bustingorry S, Savero Torres W, Gorchon J, et al. 2016. *Phys. Rev. Lett.* 117:057201
65. Ioffe LB, Vinokur VM. 1987. *Journal of Physics C: Solid State Physics* 20:6149–6158
66. Nattermann T. 1987. *Europhysics Letters (EPL)* 4:1241–1246
67. Vinokur VM, Marchetti MC, Chen LW. 1996. *Phys. Rev. Lett.* 77:1845–1848
68. Anderson PW, Kim YB. 1964. *Rev. Mod. Phys.* 36:39–43
69. Kolton AB, Rosso A, Giamarchi T, Krauth W. 2009. *Phys. Rev. B* 79:184207
70. Drossel B, Kardar M. 1995. *Phys. Rev. E* 52:4841–4852
71. Kolton AB, Rosso A, Giamarchi T. 2005. *Phys. Rev. Lett.* 94:047002
72. Rosso A, Krauth W. 2001. *Physical Review B* 65:012202
73. Ferrero EE, Foini L, Giamarchi T, Kolton AB, Rosso A. 2017. *Phys. Rev. Lett.* 118:147208
74. Arcangelis L, Godano C, Grasso JR, Lippiello E. 2016. *to be published in Physics Report*
75. Purrello VH, Iguain JL, Kolton AB, Jagla EA. 2017. *Phys. Rev. E* 96:022112
76. Rosso A, Le Doussal P, Wiese KJ. 2009. *Physical Review B* 80:144204
77. Purrello VH, Iguain JL, Kolton AB. 2019. *Phys. Rev. E* 99:032105
78. Ferrero EE, Foini L, Giamarchi T, Kolton AB, Rosso A. 2019. Non-linear elasticity and collective events in domain wall creep dynamics. In preparation
79. Gorchon J, Bustingorry S, Ferré J, Jeudy V, Kolton AB, Giamarchi T. 2014. *Phys. Rev. Lett.* 113:027205
80. Cao X, Bouzat S, Kolton AB, Rosso A. 2018. *Phys. Rev. E* 97:022118
81. Diaz Pardo R, Savero Torres W, Kolton AB, Bustingorry S, Jeudy V. 2017. *Phys. Rev. B* 95:184434
82. Caballero NB, Fernández Aguirre I, Albornoz LJ, Kolton AB, Rojas-Sánchez JC, et al. 2017. *Phys. Rev. B* 96:224422
83. Jeudy V, Díaz Pardo R, Savero Torres W, Bustingorry S, Kolton AB. 2018. *Phys. Rev. B*



- 98:054406
84. Grassi MP, Kolton AB, Jeudy V, Mougín A, Bustingorry S, Curiale J. 2018. *Phys. Rev. B* 98:224201
  85. Herrera Diez L, Jeudy V, Durin G, Casiraghi A, Liu YT, et al. 2018. *Phys. Rev. B* 98:054417
  86. Domenichini P, Quinteros CP, Granada M, Collin S, George JM, et al. 2019. *Phys. Rev. B* 99:214401
  87. Shahbazi K, Kim JV, Nembach HT, Shaw JM, Bischof A, et al. 2019. *Phys. Rev. B* 99:094409
  88. Larkin AI, Ovchinnikov YN. 1979. *Journal of Low Temperature Physics* 34:409–428
  89. Nattermann T, Shapir Y, Vilfan I. 1990. *Phys. Rev. B* 42:8577–8586
  90. Démercy V, Lecomte V, Rosso A. 2014. *Journal of Statistical Mechanics: Theory and Experiment* 2014:P03009
  91. Shibauchi T, Krusin-Elbaum L, Vinokur VM, Argyle B, Weller D, Terris BD. 2001. *Phys. Rev. Lett.* 87:267201
  92. Moon KW, Kim DH, Yoo SC, Cho CG, Hwang S, et al. 2013. *Phys. Rev. Lett.* 110:107203
  93. Pardo RD, Moisan N, Albornoz L, Lemaitre A, Curiale J, Jeudy V. 2019. Common universal behaviors of magnetic domain walls driven by spin-polarized electrical current and magnetic field
  94. Clemmer JT, Robbins MO. 2019. *Phys. Rev. E* 100:042121
  95. Zhou NJ, Zheng B. 2014. *Phys. Rev. E* 90:012104
  96. Repain, V., Bauer, M., Jamet, J.-P., Ferré, J., Mougín, A., et al. 2004. *Europhys. Lett.* 68:460–466